Microporous and Mesoporous Materials 305 (2020) 110361

Contents lists available at ScienceDirect

Microporous and Mesoporous Materials

journal homepage: http://www.elsevier.com/locate/micromeso

Entrapped NbO_x clusters in MFI zeolite for sustainable acid catalysis

Enhui Yuan [a,b], Weili Dai [b], Guangjun Wu [b], Naijia Guan [b], Landong Li [b,*]

[a] School of Chemistry & Chemical Engineering, Shaanxi Normal University, Xi'an, 710119, Shaanxi Province, PR China
[b] School of Materials Science and Engineering & National Institute for Advanced Materials, Nankai University, Tianjin, 300350, PR China

ARTICLE INFO

Keywords:
NbO_x clusters
MFI zeolite
Solid Lewis acid
Cross-aldol condensation

ABSTRACT

Entrapping the small NbO_x clusters into MFI zeolite crystals was directly prepared via a facile hydrothermal method, assisting with the sodium citrate and EDTA-2Na to dissolve and chelate the niobium precursors. The existing states and configurations of Nb species in the zeolites were carefully characterized by a series of techniques including XRD, FTIR, SEM, TEM, UV–Vis, XPS and Raman. These results clearly indicated that the entrapped oligomeric NbO_x clusters in MFI zeolite crystals contained Nb-OH, Nb=O and Nb-O-Si bonds. These characters were the origin of both Lewis and Brønsted acid sites for these Nb-MFI samples, which was vividly confirmed by FTIR spectroscopy with pyridine absorption and solid-state NMR spectroscopy with ammonia and TMPO as probing molecules techniques. The as-prepared Nb-MFI zeolites were employed as sustainable Lewis acids in several catalytic reactions. Especially, Nb-MFI zeolites exhibited remarkable catalytic performance in the cross-aldol condensation between furfural and acetone for biomass upgrading, surpassing traditional Lewis acidic zeolites Sn-MFI and Sn-BEA in terms of activity and selectivity, respectively. The 2.6%Nb-MFI also showed very good stability during reaction and it could be recycled for six times without loss in activity. Finally, 2.6%Nb-MFI was verified as a general catalyst for the cross-aldol condensation reaction between small-molecule aldehydes and ketones. All these results demonstrate the great potential of Nb-MFI as a robust catalyst for the shape-selective Lewis acid catalysis. The synthesis strategy developed herein could be readily extended to the construction of zeolite entrapped high-valence transition metal clusters for catalytic applications.

These authors declared that they have no conflicts of interest to this work.

1. Introduction

The high-valance transition metals containing zeolites, such as W-MFI, Mo-MFI and V-TON, are recently attracting significant attention due to their unique properties in various applications [1–4]. Especially, the high-valance transition metals containing zeolites exhibit remarkable catalytic properties, which could be ascribed to the versatile characteristics of the high-valance transition metals, the molecular-sized skeleton structure of zeolites and their subtle interactions [5]. It is highly desirable to explore and construct more types of high-valance transition metals containing zeolites for potential catalytic applications. The hydrated form of niobium pentoxide $Nb_2O_5 \bullet nH_2O$, also known as niobic acid, possesses both Lewis and Brønsted acidity (associated with the Nb=O and Nb-OH bonds, respectively) and it has been widely applied as solid acids in various reactions [6–8]. Generally, Nb species are dispersed and stabilized on a certain support with large surface area, e.g. mesoporous silica, to make better use of the active Nb species, and such type of supported materials have been successfully applied as good catalysts in the hydration of epoxides, the Meerwein-Ponndorf-Verley reduction of aldehydes and ketones with alcohol, the epoxidation of olefin by H_2O_2 and etc. [9–12] Thereupon, it is easily imaged to entrap highly-dispersed Nb species in zeolite matrix, i.e. Nb-containing zeolites, to generate distinctive properties for some specific reactions. Nb-containing zeolites can be prepared via direct hydrothermal synthesis and post-synthesis modifications. In early studies, Nb-containing zeolites e.g. Nb-BEA, Nb-FAU and Nb-MFI, are synthesized via the direct hydrothermal approach using niobium pentaethoxide as the Nb precursor [13–16]. Niobium pentaethoxide is expensive and very sensitive to the moisture, which make the synthesis costly and complex. Certain Nb-containing zeolite, i.e. Nb-BEA, has been successfully prepared via the post-synthesis modification approach [17], which involves a large amount of concentrated nitric acid to dealuminate the parent BEA zeolite and raises serious safety and environment concerns. Despite

* Corresponding author.
E-mail address: lild@nankai.edu.cn (L. Li).

https://doi.org/10.1016/j.micromeso.2020.110361
Received 16 April 2020; Received in revised form 21 May 2020; Accepted 22 May 2020
Available online 20 June 2020
1387-1811/

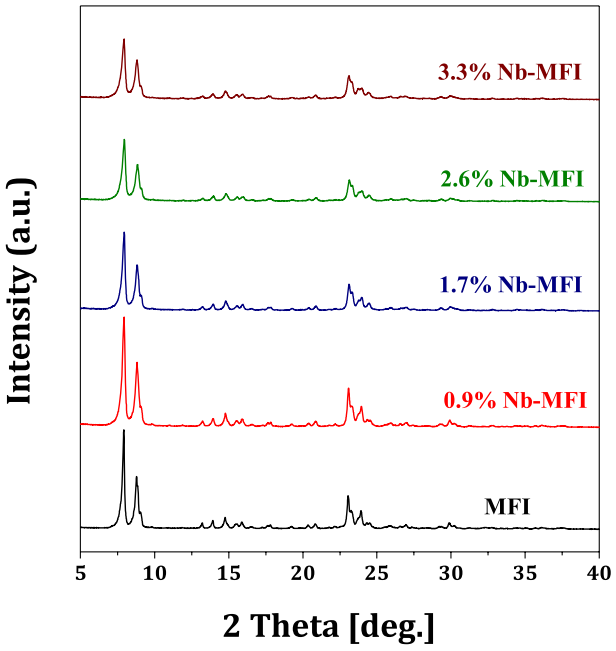

Fig. 1. XRD patterns of the as-prepared siliceous MFI and Nb-MFI with different Nb loadings.

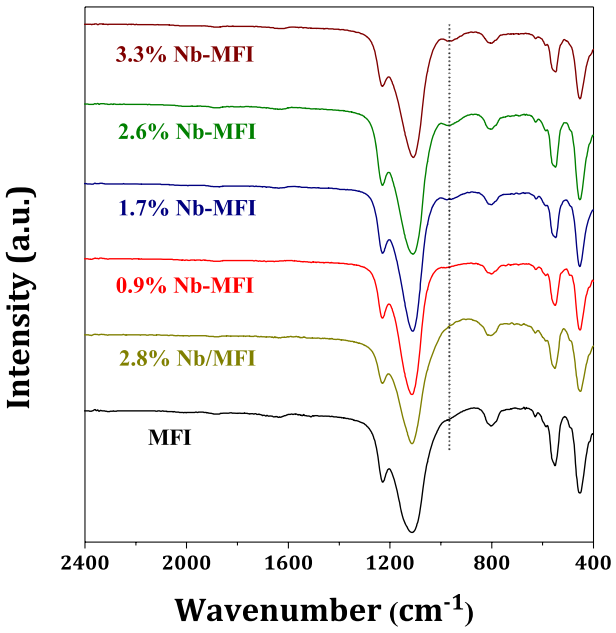

Fig. 2. FTIR spectra of siliceous MFI, Nb-MFI with different Nb loadings and 2.8%Nb/MFI.

of current achievements, the facile synthesis of Nb-containing zeolites is still challenging, which greatly limits their catalytic applications. Meanwhile, although the existing states of Nb species in zeolite have been investigated via different techniques, it is unclear whether the Nb species have been incorporated into zeolite framework or locate at the extraframework positions in the form of NbO_x clusters. Accordingly, the origin of activity in Nb-containing zeolites and the structure-activity relationship in certain reaction is unavailable.

The aldol condensation is an important reaction for C-C bond coupling to synthesis value-added organics and it has triggered broad interests in the past decades [18–20]. Typically, the cross-aldol reaction between furfural and acetone has been developed to produce long-chain fuel precursors. A proposed reaction mechanism is that the strong basic catalysts can induce the abstraction of the α-protons from the acetone molecules and generate enolate intermediates for the formation of C-C bonds [21–23]. Homogenous bases like NaOH have been widely applied in the aldol condensation process, while these homogenous bases unavoidably suffer from several key drawbacks, i.e. the strong corrosion to the reactor, the unrecyclability and large amounts of alkaline waste water generated [24]. Heterogeneous bases like MgO can also catalyze the aldol condensation reaction, but they are not tolerant to the water and hard to recycle [25,26]. The Lewis acidic zeolites are recently reported to be alternative catalysts for the activation of carbonyl-containing molecules and they can promote the cross-aldol reaction between aldehydes and ketones for the direct C-C bond formation [21,27–30]. In this context, the high-valance transition metals containing zeolites like Nb-containing zeolites might be good candidates to catalyze the reaction, which is yet not fully investigated.

Herein, we develop a direct hydrothermal synthesis route to Nb-containing MFI zeolite using niobiumoxalate as the Nb precursor and in the presence of sodium citrate and disodium ethylenediamine tetraacetate (EDTA-2Na). During the synthesis, the niobiumoxalate well dissolves in the sodium citrate solution, and the EDTA-2Na readily chelates the soluble Nb species and formation of Nb-containing complex, which completely avoiding the formation of insoluble niobium oxides. The Nb-containing complex is facilely encapsulated into the MFI zeolite crystals when it directly added into the gel of MFI zeolite synthetic precursors. The entrapped ultrafine NbO_x clusters MFI zeolites are vividly obtained through calcination of the as-prepared zeolites. Comprehensive characterization results reveal that NbO_x clusters are highly entrapped in the siliceous MFI zeolite crystals, which give rise to both Lewis and Brønsted acidity. The as-obtained Nb-containing MFI zeolites are applied as efficient heterogeneous catalysts in the cross-aldol condensation between furfural and acetone, an important reaction of biomass upgrading. Our results provide a facile strategy to high-valance transition metals containing zeolites as robust solid acids for catalytic applications.

2. Experimental section

2.1. Synthesis of Nb-MFI zeolites

The Nb-MFI zeolites with different Nb loadings were carefully synthesized via a direct hydrothermal method with niobiumoxalate as the Nb precursor in the presence of disodium ethylenediamine tetraacetate (EDTA-2Na) and sodium citrate. In a typical synthesis, 0.66 g of NaOH, 21.2 g of tetrapropylammonium hydroxide aqueous (TPAOH, 25 wt% in water) and 30 g of H_2O were well mixed to form a transparent liquid, and then 6.30 g fumed silicon was cautiously added under stirring. The mixture was stirred at 60 °C for 8 h and denoted as solution **A**. Meanwhile, 0.52 g of EDTA-2Na and 3.0 g of sodium citrate dehydrate were dissolved in 20 g of H_2O under stirring at 80 °C and denoted as solution **B**. The liquid containing 0.68 g of niobium oxalate hexahydrate and 20 g of H_2O was dropwise added in the solution **B** and the formed clear liquid was denoted as solution **C**. The solution **C** was slowly added into the solution **A** and stirred at 60 °C for 3 h. Finally, the liquid mixture was transferred into a 100 mL Teflon-lined autoclave and crystallized at 200 °C for 3 days. The solid product was collected by centrifugation, thoroughly washed with deionized water, dried at 80 °C for 24 h, and calcined in flowing air at 550 °C for 6 h. The calcined product was ion-exchanged with 6 wt% NH_4Cl aqueous solution at 80 °C for 4 h, filtrated, washed and dried at 80 °C for 12 h. The final product was obtained by calcination the above treated sample in flowing air at 550 °C for 6 h, and labeled as Nb-MFI. To obtain Nb-MFI zeolites with different Nb loadings, the molar composition of the batch was controlled as $1SiO_2/0.06Na_2O/0.25TPAOH/(0.006–0.015)Nb_2O_5/45H_2O$. The Nb-MFI zeolites with different Nb loadings were denoted as wt.% Nb-MFI, where the wt.% represented the actual Nb loading measured by inductive coupled

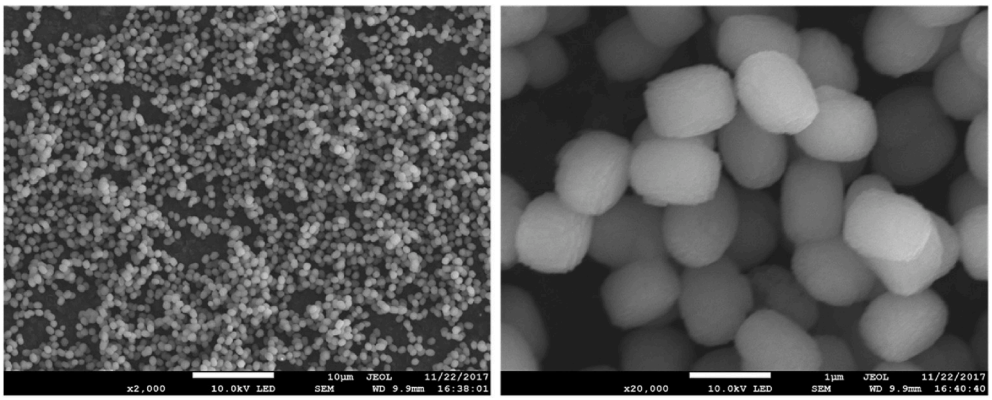

Fig. 3. SEM images of the as-synthesized 2.6% Nb-MFI zeolite.

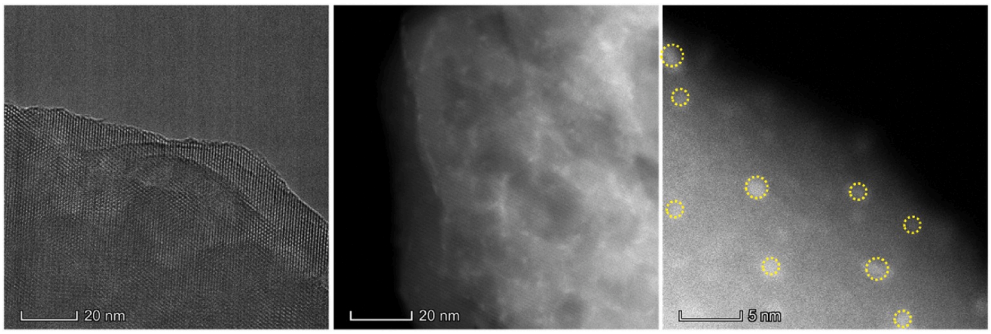

Fig. 4. HR-TEM and HAADF-STEM images of the as-synthesized 2.6% Nb-MFI zeolite.

plasma optical emission spectroscopy (ICP-OES).

For reference, the Nb supported on silicate-1, i.e. Nb/MFI, was also prepared by wetness impregnation. Typically, 0.35 g of niobium oxalate hexahydrate and 2.0 g of silicate-1 was added to 40 g of H_2O at room temperature and stirred for 1 h. Then the reaction mixture was heated to and kept at 60 °C until the water was completely evaporated. The left solid were transferred to a muffle and calcined in flowing air at 550 °C for 6 h.

2.2. Characterization techniques

The X-ray diffraction patterns of samples were collected on Bruker D8A25 diffractometer with Cu Kα radiation (λ = 1.54184 Å) and operated at 40 kV and 30 mA.

The nitrogen adsorption-desorption isotherms of zeolite samples were recorded on a QuantachromeiQ-MP gas adsorption analyzer. Before tests, all the samples were degassed at 673 K for 8 h.

The morphology of zeolite samples was observed by a field emission scanning electron microscope (SEM, JEOL JSM-6700 F).

Transmission electron microscopy (TEM) images and high angle annular dark filed (HAADF) images were acquired on a FEI Themis Z electron microscope operated at an accelerating voltage of 300 kV. Mapping the elemental distribution of samples was conducted under HAADF-STEM (scanning transmission electron microscopy) mode using a FEI built-in energy dispersive spectrum (EDS) software.

The Fourier transform infrared (FTIR) spectra of samples were recorded on a Nicolet Nexus 870 spectrometer at 4 at a resolution of 2 cm^{-1} with KBr as the background.

The diffuse reflectance ultraviolet–visible (UV–vis) spectra of dehydrated samples were recorded on a PerkinElmer Lambda 750 UV–Vis–NIR spectrophotometer with $BaSO_4$ as the background.

X-ray photoelectron spectra (XPS) Nb-containing MFI zeolites were recorded on a Thermo Scientific ESCALAB 250Xi spectrometer using monochromatic Al-K_α X-ray as the excitation source. Accurate binding energies (±0.1 eV) were determined with respect to the position of the adventitious C 1s peak at 284.8 eV.

The Raman spectra of dehydrated samples were recorded on a high-resolution, RTS-B Raman system excited by Nd:YAG laser (532 nm, output power of 50 mW).

The temperature programmed desorption of ammonia (NH_3-TPD) was conducted on an AutoChem II 2920 instrument. In a typical experiment, the sample was loaded in a quartz tube and preheated at 600 °C in He. After cooled down to 80 °C, the sample was saturated with 10% NH_3/He and then purged with He at the same temperature to eliminate the physically absorbed NH_3, The NH_3-TPD signals were recorded in the flowing He at a rate of 10 °C/min from 80 to 650 °C.

The experiments of FTIR spectroscopy with pyridine absorption were conducted on the Bruker Tensor 27 spectrometer and the detailed operational information could be found in our previous work [29].

The magic angle spinning nuclear magnetic resonance (MAS NMR) experiments were performed on a Bruker Avance III spectrometer at resonance frequencies of 400.1, 161.9 MHz for ^1H, ^{31}P nuclei, respectively. The detailed procedures can be referred to our previous work [29, 30].

2.3. Catalytic evaluations

The typical cross-aldol condensation reaction between furfural and acetone was conducted in a 15 mL stainless-steel autoclave. The main procedures were as follows: 1.25 mmol of furfural, 12.5 mmol of acetone and 0.25 mmol of mesitylene (internal standard) were homogenously mixed at room temperature, and then 100 mg of zeolite catalyst was quickly added in the stainless-steel autoclave. The autoclave was subsequently sealed and rapidly heated to 120 °C after feeding 1.0 MPa N_2. After reaction for a period of time, the solid catalyst was removed by centrifugation and the liquid phase was diluted with acetone and

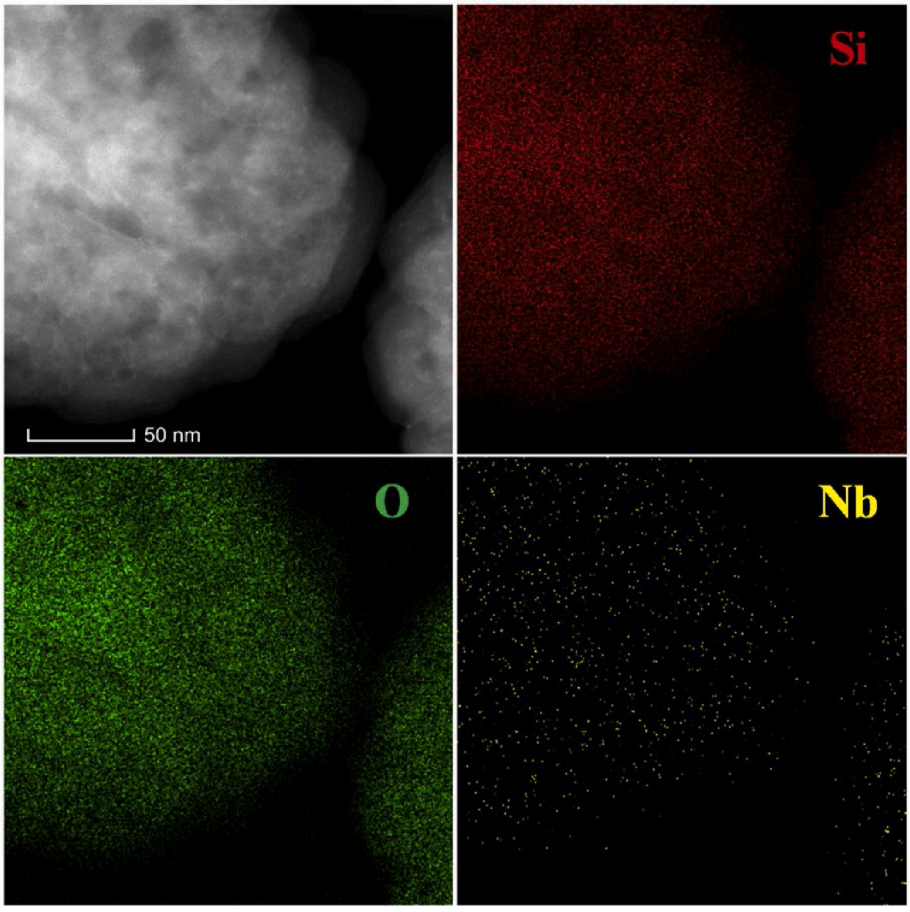

Fig. 5. STEM image and elemental maps of the as-synthesized 2.6% Nb-MFI zeolite.

Table 1
Physico-chemical properties of Nb-MFI zeolites with different Nb loadings.

Sample	Nb Loading		Si/Nb[a]	S_{BET} (m^2/g)	V_{micro} (m^3/g)
	Target	Actual[a]			
0.9% Nb-MFI	1.0	0.9	170	397	0.15
1.7% Nb-MFI	2.0	1.7	90	382	0.14
2.6% Nb-MFI	3.0	2.6	60	380	0.14
3.3% Nb-MFI	4.0	3.3	45	375	0.13

[a] Determined by ICP.

analyzed through the Shimadzu 2010 GC (Agilent HP-5 MS column, 30 m × 0.25 mm × 0.25 μm; FID detector).

For the recycling experiment, the used catalysts were washed with acetone for several times, dried at 80 °C for 12 h and calcined in flowing air at 500 °C for the next run.

3. Results and discussion

3.1. Successful synthesis of Nb-MFI zeolites

The XRD patterns of the as-prepared siliceous MFI and Nb-MFI samples are shown in Fig. 1. All samples exhibit typical MFI structures with good crystallinity, demonstrating the successful synthesis of these samples [31]. In Fig. 2, the FTIR spectra of these samples also reveal the formation of MFI zeolites. Specifically, the well-defined peaks at 450, 550, 795 and 1110 cm^{-1}, due to the Si-O bending vibration, the pentasil framework vibration, Si-O-Si symmetric vibration and asymmetric vibration, respectively, are observed [32,33]. Notably, an obviously vibration band at 965 cm^{-1} occurs in Nb-MFI samples (not observed in

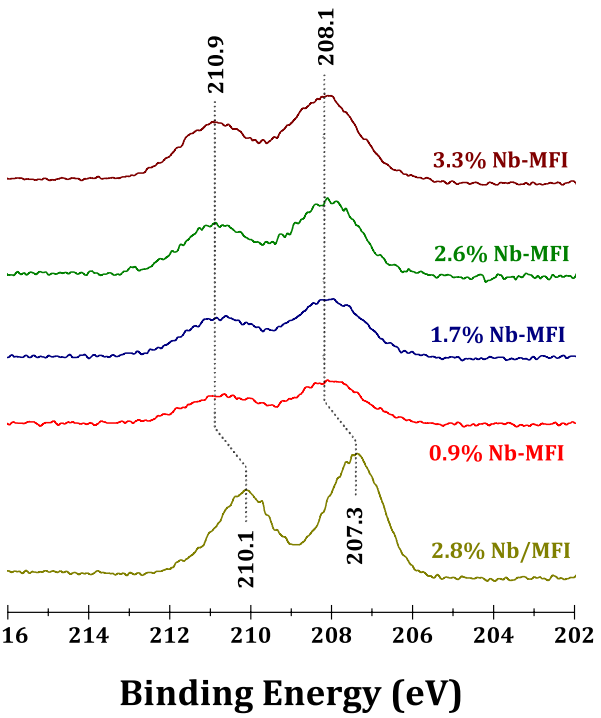

Fig. 6. Nb 3d XPS of Nb-MFI with different Nb loadings and 2.8%Nb/MFI.

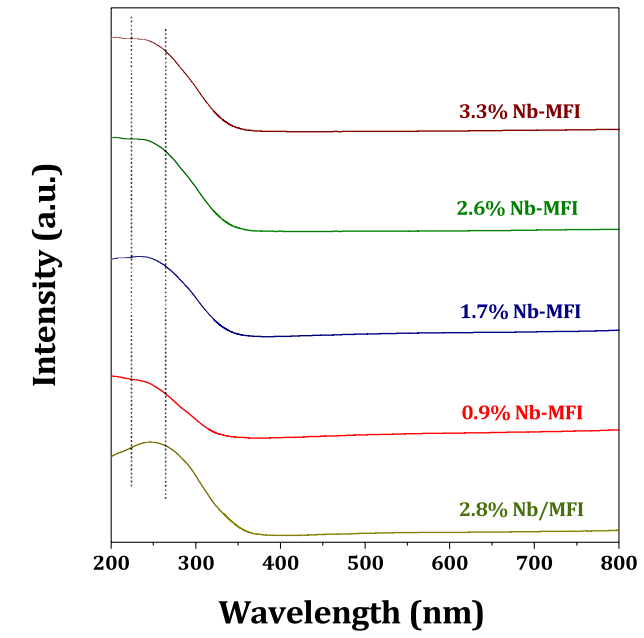

Fig. 7. UV–vis spectra of Nb-MFI with different Nb loadings and 2.8%Nb/MFI.

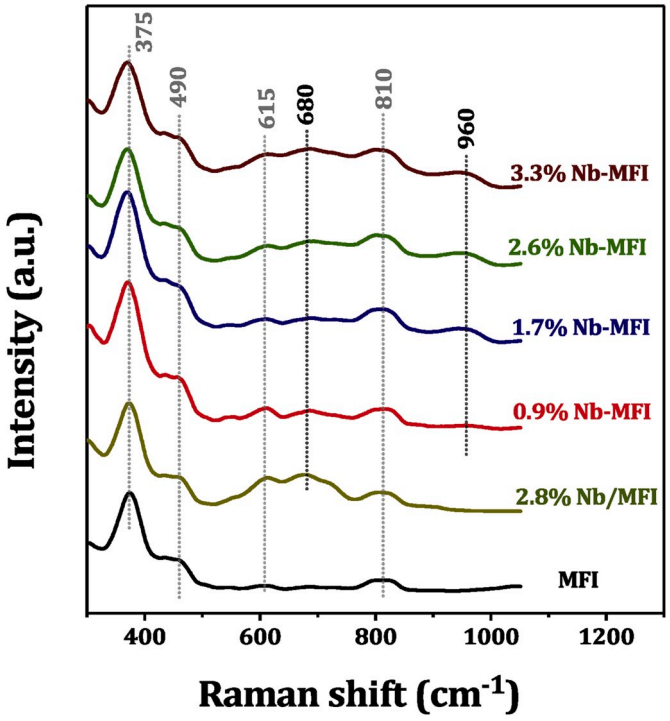

Fig. 8. Raman spectra of siliceous MFI, Nb-MFI with different Nb loadings and 2.8%Nb/MFI.

MFI and Nb/MFI samples) and its intensity increases with increasing Nb loadings. This band is now unambiguously ascribed to Si-OH groups, a type of defects in MFI zeolite [34–36]. The presence of Si-OH groups is also directly confirmed by the FTIR spectra of hydroxyl stretching region (Fig. S1), while other types of hydroxyls like Nb-OH-Si or Nb-OH could not be distinguished due to the spectroscopy overlap by Si-OH groups. The formation of Si-OH defects in MFI zeolites upon Nb introduction might indicate the strong interaction between Nb species and zeolite framework, which also results in the decline in the relative crystallinity of MFI zeolites as observed in the XRD patterns (Fig. 1). According to

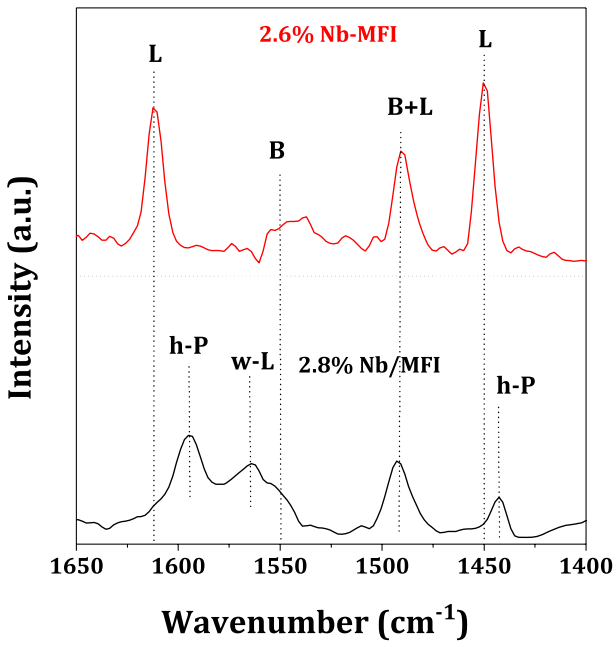

Fig. 9. FTIR spectra of pyridine adsorption on 2.8% Nb/MFI and 2.6% Nb-MFI samples.
L, B, B
+
L, w-L and h-P represents the strong Lewis acid-bonded pyridine molecules, pyridinium ions on Brønsted acid site, pyridine molecules associated with Brønsted and/or Lewis acid sites, weak Lewis acid-bonded pyridine molecules and hydrogen bonded-pyridine molecules, respectively.

these results, we can say that the Nb species are stabilized by the Si-OH defects in MFI zeolites.

The SEM images of all Nb-MFI samples show isolated and uniform ellipsoids with an approximate diameter of 0.5 μm, and the representative SEM images of 2.6%Nb-MFI are shown in Fig. 3 for reference. The high resolution TEM image (Fig. 4, left-chart) of 2.6%Nb-MFI reveals the clear lattice fringes of MFI zeolite, corresponding to the high crystallinity of the sample. No Nb-containing species could be distinguished in the TEM image. While in the HAADF-STEM image (Fig. 4, middle-chart), the presence of tiny Nb-containing particles (the bright points) can be clearly seen. The apparent sizes of these particles are determined to be 1–2 nm (Fig. 4, right-chart), small enough to be called as clusters. That is, Nb-containing clusters, i.e. NbO_x clusters, are entrapped in MFI zeolite crystals for the sample of 2.6%Nb-MFI. The homogeneous distribution of Nb species within zeolite matrix is further confirmed by STEM elemental mapping analysis. As shown in Fig. 5, very good dispersion of Nb species with sizes below 2 nm in 2.6%Nb-MFI zeolites can be clearly observed, in significant contrast to 2.8%Nb/MFI (Fig. S2). The texture properties of the as-prepared Nb-MFI zeolites are characterized by means of low temperature nitrogen physisorption and the results are summarized in Table 1. Both the specific surface area and the microporous volume of Nb-MFI zeolites slightly decrease with the increasing Nb loadings. Nevertheless, the specific surface area (>375 m^2/g) and the total pore volume (>0.13 m^3/g) are comparable with commercial MFI zeolites.

3.2. *The existing states of Nb species in MFI zeolite*

According to the characterization results from XRD, FTIR and microscopy, we can say that Nb-containing clusters have been successfully confined in MFI zeolite via our direct hydrothermal strategy. Subsequently, the existing states of Nb species in zeolite are investigated by several complementary spectroscopic techniques.

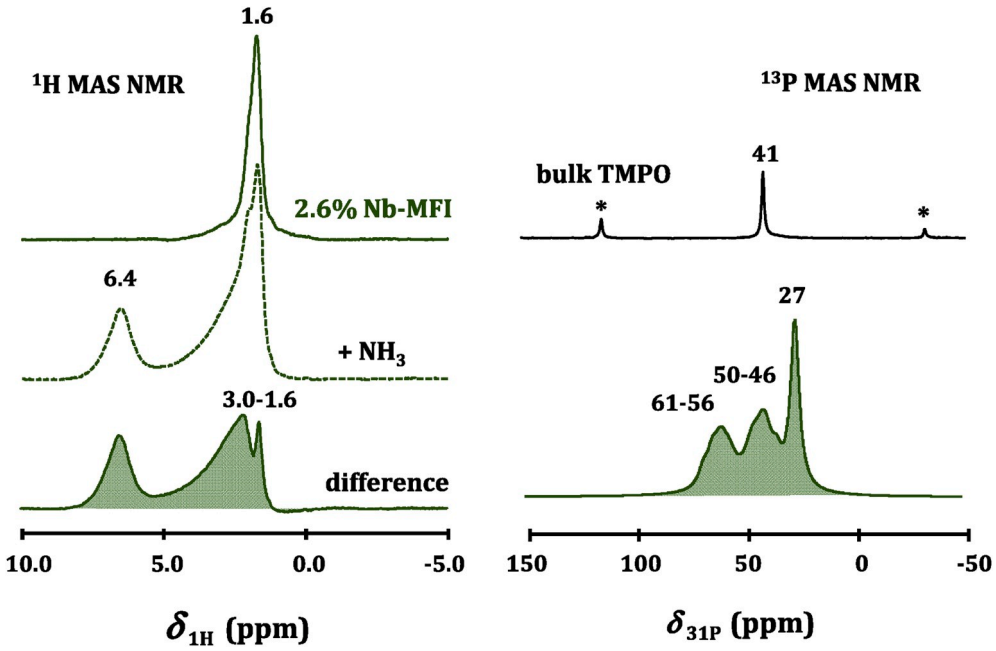

Fig. 10. ^{1}H MAS NMR spectra of ammonia adsorption (left) and ^{31}P MAS NMR spectra of trimethylphosphine oxide (TMPO) adsorption on 2.6% Nb-MFI zeolite (right).

Table 2
The cross-aldol condensation between furfural and acetone on Nb-MFI catalysts with different Nb loadings[a].

Catalyst	Conversion (%)	Selectivity (%)	Reaction rate[e] (mmol $h^{-1}g_{cat}^{-1}$)	Reference
No	<1	/	/	This work
Siliceous MFI	<1	/	/	This work
0.9% Nb-MFI[b]	19.9	99.9	1.24	This work
1.7% Nb-MFI[b]	37.8	99.9	2.36	This work
2.6% Nb-MFI[b]	51.8	99.9	3.24	This work
3.3% Nb-MFI[b]	51.2	99.9	3.20	This work
2.8% Nb/MFI[b]	10.8	99.9	0.68	This work
2.6% Nb-MFI[c]	14.6	99.9	1.50	This work
2.6% Nb-MFI[d]	70.3	95.6	4.38	This work
Sn-MFI[d]	57.0	82.4	3.56	[28]
Sn-BEA[d]	100	40.0	6.25	[28]
Sn-MFI[c]	16.2	98.9	1.01	[29]
Sn-Al-MFI[c]	17.0	98.7	1.06	[29]

[a] Reaction conditions: 1.25 mmol furfural, 12.5 mmol acetone, 0.1 g catalyst, 1 MPa N_2, time = 2 h.
[b] Temperature = 140 °C.
[c] Temperature = 120 °C.
[d] Temperature = 160 °C.
[e] The reaction rates were calculated from the results with 2 h.

The Nb 3d XPS of Nb/MFI and Nb-MFI with different Nb loadings are presented in Fig. 6. The binding energy values at 207.3 and 210.1 eV are observed for Nb/MFI, corresponding to $3d_{5/2}$ and $3d_{3/2}$ peak of niobium pentoxide, respectively [37,38]. While for Nb-MFI, similar $3d_{5/2}$ and $3d_{3/2}$ binding energy values at 208.1 eV and 210.9 eV, respectively, are observed, distinctly higher (~0.8 eV) than those for Nb/MFI or niobium pentoxide. According to these results, the Nb species in Nb-MFI should exist in the form of Nb(V), and the shifts toward high binding energy values further reveal the strong electronic interaction between Nb species and zeolite matrix. That is, the electrons transfer from Nb to zeolite matrix via the Si-O-Nb bonds. Especially, the differentiate of Nb $3d_{5/2}$ and $3d_{3/2}$ binding energy for the Nb-MFI and Nb/MFI vividly indicate that the difference configurations of Nb species in these samples.

The UV–vis spectra of the Nb-MFI and Nb/MFI are shown in Fig. 7. An obvious absorption band at 220 nm can be identified for Nb-MFI zeolites and its intensity gradually increases with the increasing Nb loadings from 0.7 to 2.6%. The band is attributed to the charge transfer transitions from O^{2+} to tetrahedral Nb^{5+} in NbO_4 tetrahedral units [15,17]. Meanwhile, an absorption with maximum at 270 nm is observed for the 2.8%Nb/MFI and 3.3%Nb-MFI samples, which should be ascribed to the $O^{2+}\rightarrow Nb^{5+}$ charge transfer transitions in oligomeric NbO_x species [39]. For all samples, no hints on the formation of bulk Nb_2O_5 (E_g = 3.1 eV) are observed.

Raman is a very useful technique to determine the configuration of high-valence transition metal species dispersed on various supports. In this work, the dehydrated Nb-MFI and Nb/MFI samples are excited by green laser at 532 nm and their Raman responses are shown in Fig. 8. The Raman bands at 375, 490, 615 and 810 cm^{-1} are due to the Si-O-Si symmetrical stretching and bending modes [40,41], which are observed for all zeolite samples. Besides, a dominant Raman band at 680 cm^{-1} is observed for Nb/MFI, which should be attributed to the Nb-O-Nb stretching modes of different niobium oxides polyhedral [42,43]. For Nb-MFI with Nb loadings of 1.7–3.3%, clear Raman bands at 955 cm^{-1} due to the symmetric stretches of Nb=O bonds can be distinguished [40–42]. According to the Raman analyses, the introduction of similar amount of Nb species into MFI zeolite via different strategies, i.e. direct hydrothermal synthesis (2.6%Nb-MFI) and wet impregnation (2.8% Nb/MFI), results in quite different NbO_x configurations, which should be related to the interaction between NbO_x and zeolite matrix.

3.3. Acidity of Nb-MFI zeolites

The acidity of Nb-MFI and Nb/MFI zeolites is firstly examined by the NH_3-TPD and the results are shown in Fig. S3. The Nb-MFI samples show attractive acidity and the acidity density (revealed by the amount of ammonia desorbed per mass of sample) gradually increases with increasing Nb loadings. It is interesting to note that the acidity density of

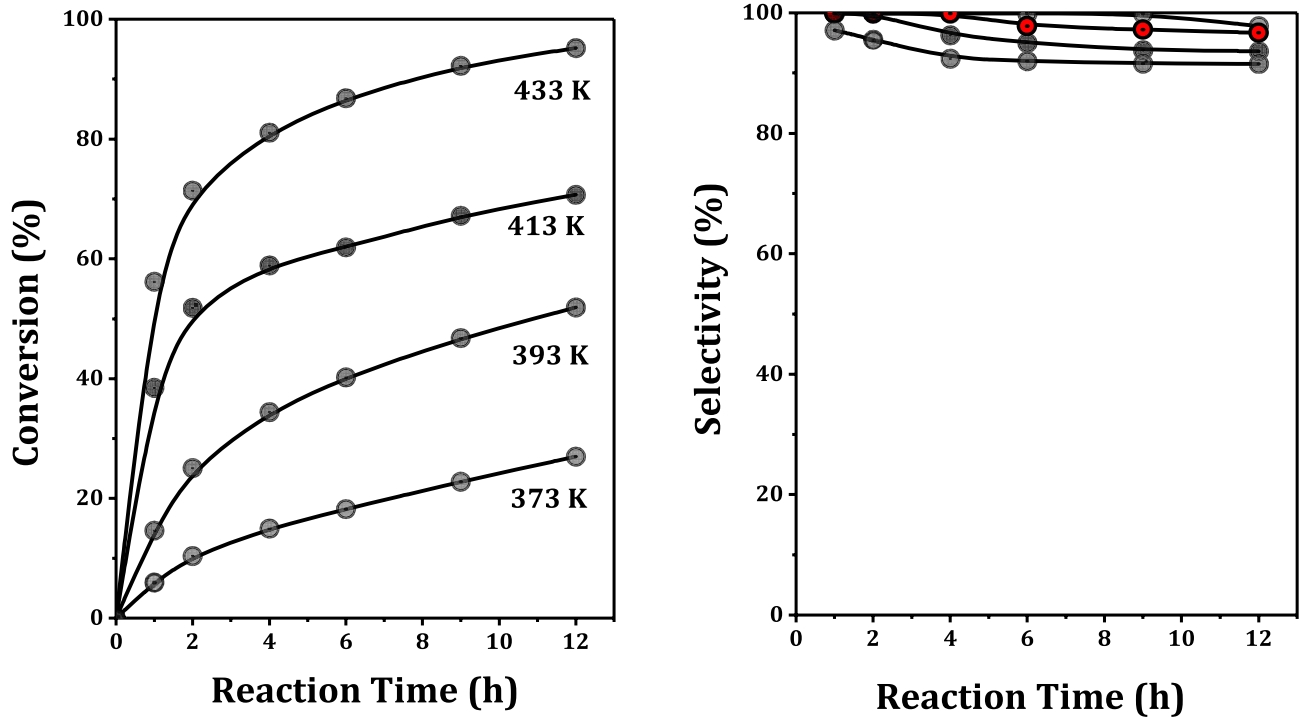

Fig. 11. Time-dependent furfural conversion and furfurylideneacetone selectivity at different temperatures. Reaction conditions: 1.25 mmol furfural, 12.5 mmol acetone, 0.1 g catalyst, 1 MPa N_2.

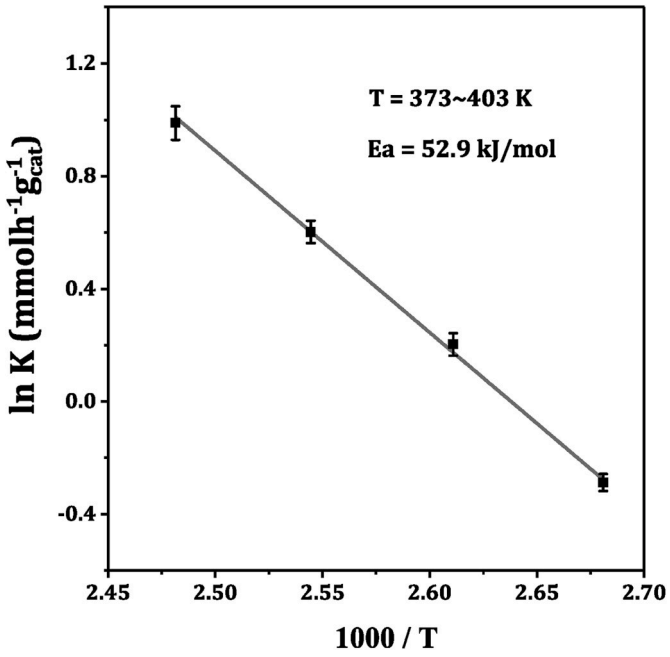

Fig. 12. Kinetic plots of furfural and acetone cross-aldol condensation catalyzed by 2.6% Nb-MFI zeolites. Reaction conditions: 1.25 mmol furfural, 12.5 mmol acetone, 0.1 g catalyst, 1 MPa N_2.

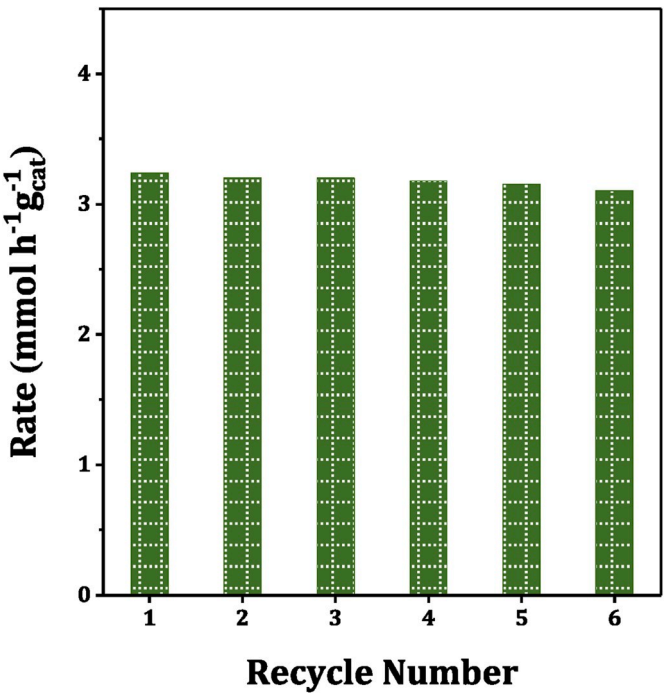

Fig. 13. Recycling test of 2.6% Nb-MFI in the cross-aldol condensation of furfural and acetone. Reaction conditions: 1.25 mmol furfural, 12.5 mmol acetone, 0.1 g catalyst, 1 MPa N_2; temperature = 140 °C, time = 2 h.

2.6%Nb-MFI is much higher than that of 2.8%Nb/MFI with similar Nb loading. Considering that the acidity of Nb-MFI and Nb/MFI both comes from the Nb species, the much higher acidity density of Nb-MFI can be explained from the high dispersion of NbO_x species for acidity generation, as supported by electroscope observation (Figs. 4 and 5) and Raman analysis (Fig. 8).

To reveal the nature of acid sites in Nb-MFI and Nb/MFI samples, experiments of FTIR spectroscopy with pyridine adsorption are conducted (Fig. 9). Generally, the IR bands of pyridine centered at different wavenumbers indicate specific adsorbed pyridines on the measured substrate. The FTIR spectrum of pyridine absorption on Nb-MFI shows several bands that can be attributed to strong Lewis acid-bonded pyridine molecules (1610 and 1450 cm^{-1}), pyridinium ions on Brønsted acid

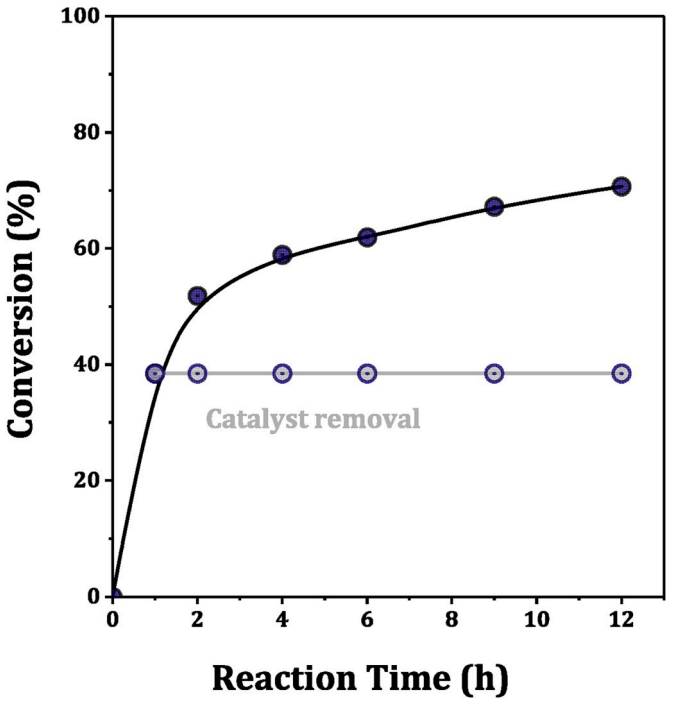

Fig. 14. Time-dependent furfural conversion in the cross-aldol condensation with catalyst removal by hot filtration. Reaction conditions: 1.25 mmol furfural, 12.5 mmol acetone, 0.1 g catalyst, 1 MPa N_2; temperature = 140 °C.

sites (1550 cm^{-1} or lower), pyridine molecules associated with Brønsted and/or Lewis acid sites (1490 cm^{-1}) [44]. In contrast, the FTIR spectrum of pyridine absorption on Nb/MFI sample displays several bands assigned to hydrogen-bonded pyridine molecules (1595 and 1445 cm^{-1}) and weak Lewis acid-bound pyridine molecules (1564 cm^{-1}) [45]. The subtle differentiate of pyridine absorption modes hints the different geometries of NbO_x species in the two samples prepared by different strategies and the stronger Lewis acidity (both acid strength and density) in Nb-MFI is clearly described.

In addition, the acidity of as-prepared Nb-MFI zeolites is investigated by NMR with probe adsorption, i.e. ^1H MAS NMR with ammonia adsorption and ^{31}P MAS NMR with trimethylphosphine oxide (TMPO) adsorption. The ^1H MAS NMR spectra of 2.6%Nb-MFI before and after ammonia adsorption are showed in Fig. 10. A dominant signal at δ_{1H} = 1.6 ppm due to Si-OH at framework defects [46], together with possible shoulders due to Nb-OH, is observed for 2.6%Nb-MFI. Upon ammonia loading, the intensity of signals in the range of δ_{1H} = 1.6–3.0 ppm increases due to ammonia molecules coordinated at the Lewis acid sites and a new strong signal at δ_{1H} = 6.4 ppm emerges due to formation of protonated ammonia molecules [29,30,46]. The difference spectrum clearly reveals the existence of both Lewis acid sites (δ_{1H} = 1.6–3.0 ppm) and Brønsted acid sites (δ_{1H} = 6.4 ppm) in 2.6%Nb-MFI, which is further confirmed by ^{31}P MAS NMR spectrum with TMPO adsorption. Typically, δ_{31P} signals at 27, 46–50 and 56–61 ppm are observed for 2.6%Nb-MFI after TMPO adsorption and a preliminary evacuation (Fig. 10). The sharp signals at 27 ppm is ascribe to the "mobile" TMPO attached in the intercrystalline voids or weakly adsorbed near the channel openings of zeolites [46,47], while the signals in the region of 46–50 and 56–61 ppm are ascribed to TMPO interacting with the Lewis and Brønsted acid sites, respectively [29,30,46].

These results clearly evidence the existence of both Lewis and Brønsted acid sites in as-prepared Nb-MFI zeolites, similar to that reported for niobic acid [6]. But, the ultrasmall NbO_x species entrapped in the MFI crystal will exhibit tacit properties and it also differ from the niobic acid in the current circumstances. Summarizing all the characterization results, the presence of Nb-OH, Nb=O and Nb-O-Si bonds can be included in the NbO_x clusters confined MFI zeolite, and the possible structures are drawn in Scheme 1. Especially, the as-prepared NbO_x entrapped MFI zeolites show highly dispersed Nb species within their crystals and endows stronger Lewis acidic properties than the wetness impregnated Nb/MFI samples. The distinctive characters of Nb-MFI zeolites can create definite catalytic properties for specific acid catalyzed reactions.

3.4. Catalytic properties of Nb-MFI zeolites

According to the characterization results, Nb-MFI zeolites are solid acids with medium Lewis acidity. We then investigate the catalytic properties of Nb-MFI zeolites in the cross-aldol condensation to between furfural and acetone, a typical reaction of C-C bond construction for biomass upgrading (Scheme 2). As shown in Table 2, all Nb-MFI zeolites show high selectivity of >90% toward the target product 4-(2-furyl)-3-buten-2-one (furfurylideneacetone, FLDA) at 140 °C, and the mass specific reaction rate gradually increases with increasing Nb loading from 0.7 to 2.6%. Further increase in Nb loading from 2.6 to 3.3%, however, results in a slight decline in the mass specific reaction rate (from 3.24 to 3.20 mmol/h/g_{cat}). In contrast, 2.8%Nb/MFI exhibits very low activity with reaction rate of 0.68 mmol/h/g_{cat}, much lower than 2.6%Nb-MFI with similar Nb loading. Meanwhile, severe coking is observed with 2.8%Nb/MFI probably due to the further condensation between FLDA product with furfural to produce 1,5-bis-(2-furanyl)-1,4-pentadien-3-one and polymers, which could be greatly suppressed with

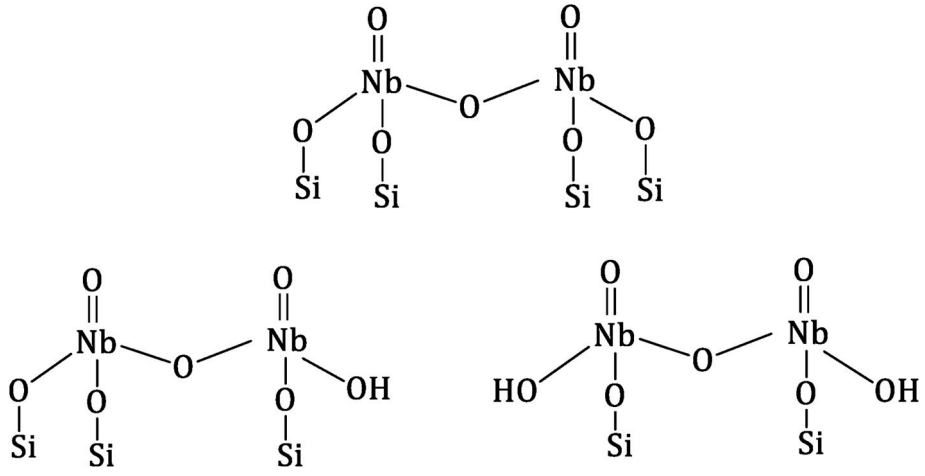

Scheme 1. Possible structures of NbO_x clusters entrapped in MFI zeolite crystals.

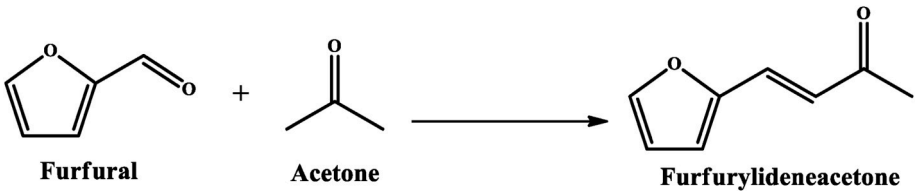

Scheme 2. The cross-aldol condensation between furfural and acetone.

NbO_x species entrapped in MFI channels, i.e. Nb-MFI. That is, although diffusion limitation does exist in Nb-MFI and shows negative effect on the reaction rate of cross-aldol condensation, it provides a good solution to suppress the secondary condensation and the coke formation thereof. Considering that siliceous MFI shows neglectable activity in the reaction (Table 2), the catalytic activity of Nb-containing zeolites should be come from Nb species and it is obviously dependent on the configurations of NbO_x.

As shown in Table 2, the as-prepared Nb-MFI zeolites also exhibit higher activity than typical Lewis acidic Sn-MFI zeolites under comparable conditions (reaction rate of 1.50 versus 1.01 mmol/h/g_{cat} at 120 °C; reaction rate of 4.38 versus 3.56 mmol/h/g_{cat} at 160 °C) [28,29]. Although Sn-BEA appears to be more active than Sn-MFI in the cross-aldol condensation reaction (reaction rate of 6.25 versus 4.38 mmol/h/g_{cat} at 160 °C) due to the diffusion advantages for the substrate molecules in its 12-membered ring channels, a very low selectivity toward the target product FLDA is obtained (~40%) and a large amount of 1,5-di-2-furanyl-1,4-pentadien-3-one (F_2PD) is detected as the by-product from secondary condensation. That is, both the reaction rate and the product selectivity in the self-aldol condensation reaction are controlled by the architecture of zeolite channels [28]. The high selectivity toward FLDA in the cross-aldol condensation between furfural and acetone catalyzed by Nb-MFI zeolites, on the other hand, indicates that the reaction occurs within MFI channels, which can be regarded as an indirect evidence for the successful entrapping of NbO_x clusters in MFI zeolite.

With 2.6%Nb-MFI zeolite as a model catalyst, the effects of reaction temperature on the cross-aldol condensation reaction are further investigated (Fig. 11). Increasing reaction temperature from 100 to 160 °C can significantly promote the reaction rate of furfural conversion but meanwhile result in a slight decline in the FLDA selectivity (especially at high furfural conversion). The apparent activation energy of the cross-aldol condensation reaction catalyzed by 2.6%Nb-MFI zeolite, according to the Arrhenius plots, is calculated to be 52.9 kJ/mol (Fig. 12),

Table 3
The cross-aldol condensation between various aldehyde and ketone substrates catalyzed by 2.6%Nb-MFI.

Entry	Substrate		Main products	Conversion (%)	Selectivity (%)
	aldehyde	Ketone			
1	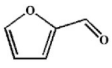		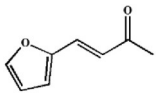	50.2	99.9
2	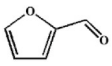	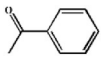	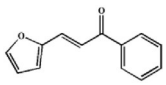	38.5	99.9
3			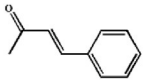	51.1	72.8
4			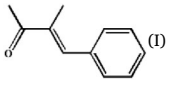 (I) 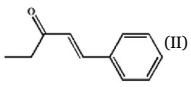 (II)	63.4	55.1 (I) 44.9 (II)
5		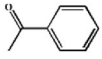	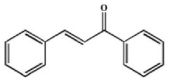	44.8	99.9
6	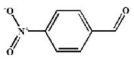		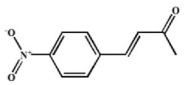	71.0	85.0
7	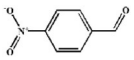	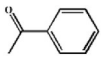	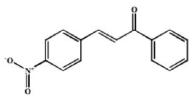	78.5	97.0
8	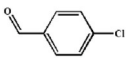		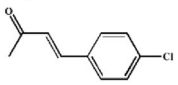	49.4	94.9
9	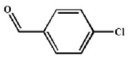	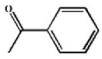	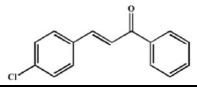	37.2	94.2

Reaction conditions: 1.25 mmol aldehyde, 12.5 mmol ketone, 0.1 g catalyst, 1.0 MPa N_2; temperature = 140 °C, time = 2 h.

which is slightly lower than that catalyzed by Sn-MFI (58.6 kJ/mol) but higher than Sn-BEA (43.9 kJ/mol) [28]. Nb-MFI zeolites are very stable during the condensation reaction, and no obvious changes can be observed after long-term run. Typically, 2.6%Nb-MFI zeolite can be recycled for six times (simple washing, drying and calcination for recycle) without loss in activity and selectivity, as shown in Fig. 13. No leaching of Nb species in the liquid phase after reaction could be detected by ICP analysis (below the detection limit of 1 ppm). The results from hot-filtration tests in Fig. 14 clearly reveal the good stability of confined NbO_x clusters in MFI zeolite during reaction and the true heterogeneity of the reaction catalyzed by Nb-MFI.

According to the above-mentioned results, Nb-MFI can be established as a robust solid acid catalyst for the cross-aldol condensation reaction between furfural and acetone. We finally investigate the substrate scope of the cross-aldol condensation catalyzed by 2.6%Nb-MFI (Table 3). It is interesting to disclose the good activity of 2.6%Nb-MFI can be achieved in the cross-aldol condensation reaction using various substrates. Typically, furfural can react with acetophenone to generate the condensation product with perfect selectivity, just like its reaction with acetone (**Entry 1&2**). The reaction rate is somewhat lower, probably due to the diffusion limit of acetophenone in the channels of MFI zeolite as compared with acetone. Benzaldehyde (**Entry 3–5**) and its derivates (**Entry 6–9**) can react with various ketones via the cross-aldol condensation pathway. In most cases, considerable reaction rate and high selectivity toward the condensation product can be achieved. The electronic/steric effects from substituting groups can well explain the different catalytic properties with different reaction substrates. Overall, 2.6%Nb-MFI is verified as a general catalyst for the cross-aldol condensation reaction between small-molecule aldehydes and ketones.

4. Conclusions

We develop herein a facile one-pot hydrothermal strategy to synthesize NbO_x entrapped MFI zeolites by using the sodium citrate solution to dissolve Nb precursor and EDTA-2Na to chelate soluble Nb species. Characterization results from XRD, FTIR, SEM, TEM, UV–Vis, XPS and Raman reveal the formation of oligomeric NbO_x clusters containing Nb-OH, Nb=O and Nb-O-Si bonds confined in MFI zeolite crystals. FTIR spectra with pyridine absorption and solid-state NMR spectra with probe adsorption, i.e. ^{1}H MAS NMR with ammonia adsorption and ^{31}P MAS NMR with TMPO adsorption, reveal the presence of both Lewis and Brønsted acid sites in the as-prepared 2.6%Nb-MFI sample, probably originated from the Nb=O and Nb-OH bonds, respectively.

The as-prepared Nb-MFI zeolites exhibit remarkable catalytic activity in the cross-aldol condensation between furfural and acetone for biomass upgrading. The optimized 2.6%Nb-MFI catalyst appears to be more active and selective than the conventional Lewis acidic zeolites Sn-MFI and Sn-BEA. 2.6%Nb-MFI also show perfect stability and recyclability in the cross-aldol condensation, demonstrating its potential for future applications. The roles of co-existing Brønsted acid sites in Nb-MFI on the Lewis acid-catalyzed cross-aldol condensation are still unclear, but at least they are not expected to play negative impacts on the reaction.

Our results indicate that the high-valence transition metal species can create catalytically active Lewis acid sites when they entrapped in zeolite crystals via chemical interaction, and they are not necessary to be incorporated into zeolite framework to generate the heteroatom-substituted zeolites in a conventional sense. Our synthesis strategy might be extended to entrap other high-valence transition metal clusters in zeolite crystals for shape-selective Lewis acid catalysis.

CRediT authorship contribution statement

Enhui Yuan: Writing - original draft. **Weili Dai:** Writing - original draft, Writing - review & editing. **Guangjun Wu:** Writing - original draft, Writing - review & editing. **Naijia Guan:** Writing - original draft, Writing - review & editing. **Landong Li:** Writing - original draft, Writing - review & editing.

Acknowledgements

We acknowledge the National Natural Science Foundation of China (21902097, 21421001), the Municipal Natural Science Foundation of Tianjin (2016YFB0701100, 18JCZDJC37400), the Postdoctoral Science Foundation of China (2019M653861XB) and the Natural Science Foundation of Shaanxi Province (2020JQ-409) for supporting the work.

Appendix A. Supplementary data

Supplementary data to this article can be found online at https://doi.org/10.1016/j.micromeso.2020.110361.

References

[1] J. Grand, S.N. Talapaneni, A. Vicente, C. Fernandez, E. Dib, H.A. Aleksandrov, G. N. Vayssilov, R. Retoux, P. Boullay, J.P. Gilson, V. Valtchev, S. Mintova, One-pot synthesis of silanol-free nanosized MFI zeolite, Nat. Mater. 16 (2017) 1010–1015.
[2] Y. Zhou, Z.P. Ma, J.J. Tang, N. Yan, Y.H. Du, S.B. Xi, K. Wang, W. Zhang, H. M. Wen, J. Wang, Immediate hydroxylation of arenes to phenols via V-containing all-silica ZSM-22 zeolite triggered non-radical mechanism, Nat. Commun. 9 (2018) 2931.
[3] P. Zhao, L. Ye, Z.Y. Sun, B.T.W. Lo, H. Woodcock, C. Huang, C. Tang, A.I. Kirkland, D.H. Mei, S.C.E. Tsang, Entrapped single tungstate site in zeolite for cooperative catalysis of olefin metathesis with Brønsted acid site, J. Am. Chem. Soc. 140 (2018) 6661–6667.
[4] F. Dubray, S. Moldovan, C. Kouvatas, J. Grand, C. Aquino, N. Barrier, J.P. Gilson, N. Nesterenko, D. Minoux, S. Mintova, Direct evidence for single molybdenum atoms incorporated in the framework of MFI zeolite nanocrystals, J. Am. Chem. Soc. 141 (2019) 8689–8693.
[5] N. Kosinov, C. Liu, E.J.M. Hensen, E.A. Pidko, Engineering of transition metal catalysts confined in Zeolites, Chem. Mater. 30 (2018) 3177–3198.
[6] K. Nakajima, Y. Baba, R. Noma, M. Kitano, J.N. Kondo, S. Hayashi, M. Hara, Nb_2O_5▪nH_2O as a heterogeneous catalyst with water-tolerant Lewis acid sites, J. Am. Chem. Soc. 133 (2011) 4224–4227.
[7] W.Q. Fan, Q.H. Zhang, W.P. Deng, Y. Wang, Niobic acid nanosheets synthesized by a simple hydrothermal method as efficient Brønsted acid catalysts, Chem. Mater. 25 (2013) 3277–3287.
[8] C. Nico, T. Monteiro, M.P.F. Graça, Niobium oxides and niobates physical properties: review and prospects, Prog. Mater. Sci. 80 (2016) 1–37.
[9] I. Nowak, Frontiers in mesoporous molecular sieves containing niobium: from model materials to catalysts, Catal. Today 192 (2012) 80–88.
[10] A. Ramanathan, R. Maheswari, D.H. Barich, B. Subramaniam, Niobium incorporated mesoporous silicate, Nb-KIT-6: synthesis and characterization, Microporous Mesoporous Mater. 190 (2014) 240–247.
[11] D.C. Tranca, A. Wojtaszek-Gurdak, M. Ziolek, F. Tielens, Supported and inserted monomeric niobium oxide species on/in silica: a molecular picture, Phys. Chem. Chem. Phys. 17 (2015) 22402–22411.
[12] M. Anilkumar, W.F. Hoelderich, A one step synthesis of caprolactam out of cyclohexanone by combined ammoximation and Beckmann rearrangement over Nb-MCM-41 catalysts, Appl. Catal. B Environ. 165 (2015) 87–93.
[13] M. Trejdaa, A. Wojtaszek, A. Floch, R. Wojcieszak, E.M. Gaigneaux, M. Ziolek, New Nb and Ta-FAU zeolites. Direct synthesis, characterization and surface properties, Catal. Today 158 (2010) 170–177.
[14] A. Corma, F.X.L. Xamena, C. Prestipino, M. Renz, S. Valencia, Water resistant, catalytically active Nb and Ta isolated Lewis acid sites, homogeneously distributed by direct synthesis in a beta zeolite, J. Phys. Chem. C 113 (2009) 11306–11315.
[15] A.M. Prakash, L. Kevan, Synthesis of niobium silicate molecular sieves of the MFI structure: evidence for framework incorporation of the niobium ion, J. Am. Chem. Soc. 120 (1999) 13148–13155.
[16] M. Hartmann, Synthesis of niobium- and tantalum-containing silicalite-1, Chem. Lett. 28 (1999) 407–408.
[17] S. Dzwigaj, Y. Millot, C. Méthivier, M. Che, Incorporation of Nb(V) into BEA zeolite investigated by XRD, NMR, IR, DR UV-vis, and XPS, Microporous Mesoporous Mater. 130 (2010) 162–166.
[18] J. Lauwaert, E.G. Moschetta, P.V.D. Voort, J.W. Thybaut, C.W. Jones, G.B. Marin, Spatial arrangement and acid strength effects on acid-base cooperatively catalyzed aldol condensation on aminosilica materials, J. Catal. 325 (2015) 19–25.
[19] D.T. Ngo, Q.H. Tan, B. Wang, D.E. Resasco, Aldol condensation of cyclopentanone on hydrophobized MgO. Promotional role of water and changes in the rate-limiting step upon organosilane functionalization, ACS Catal. 9 (2019) 2831–2841.
[20] M. Moreno-Recio, J. Santamaría-González, P. Maireles-Torres, Brönsted and Lewis acid ZSM-5 zeolites for the catalytic dehydration of glucose into 5-hydroxymethylfurfural, Chem. Eng. J. 303 (2016) 22–30.
[21] J.D. Lewis, S.V. de Vyver, Y. Roman-Leshkov, Acid-base pairs in Lewis acidic zeolites promote direct aldol reactions by soft enolization, Angew. Chem. Int. Ed. 54 (2015) 9835–9838.

[22] S.V. de Vyver, C. Odermatt, K. Romero, T. Prasomsri, Y. Roman-Leshkov, Solid Lewis acids catalyze the carbon-carbon coupling between carbohydrates and formaldehyde, ACS Catal. 5 (2015) 972–977.
[23] G.F. Liang, A.Q. Wang, X.C. Zhao, N. Lei, T. Zhang, Selective aldol condensation of biomass-derived levulinic acid and furfural in aqueous-phase over MgO and ZnO, Green Chem. 18 (2016) 3430–3438.
[24] R.E. O'Neill, L. Vanoye, C.D. Bellefon, F. Aiouache, Aldol-condensation of furfural by activated dolomite catalyst, Appl. Catal. B Environ. 144 (2014) 46–56.
[25] S.L. Yang, P.P. Huang, L. Peng, C.Y. Cao, Y.A. Zhu, F. Wei, Y.B. Sun, W.G. Song, Hierarchical flowerlike magnesium oxide hollow spheres with extremely high surface area for adsorption and catalysis, J. Mater. Chem. 4 (2016) 400–406.
[26] K.K. Zhu, J.C. Hu, C. Kobel, R. Richards, Efficient preparation and catalytic activity of MgO(111) nanosheets, Angew. Chem. Int. Ed. 118 (2006) 7435–7439.
[27] Y. Roman-Leshkov, M.E. Davis, Activation of carbonyl-containing molecules with solid Lewis acids in aqueous media, ACS Catal. 1 (2011) 1566–1580.
[28] M.X. Su, W.Z. Li, T.W. Zhang, H.S. Xin, S. Li, W. Fan, L.L. Ma, Production of liquid fuel intermediates from furfural via aldol condensation over Lewis acid zeolite catalysts, Catal. Sci. Technol. 7 (2017) 3555–3561.
[29] E.H. Yuan, W.L. Dai, G.J. Wu, N.J. Guan, M. Hunger, L.D. Li, Facile synthesis of Sn-containing MFI zeolites as versatile solid acid catalysts, Microporous Mesoporous Mater. 270 (2018) 265–273.
[30] T. Yan, W. Dai, G. Wu, S. Lang, M. Hunger, N. Guan, L. Li, Mechanistic insights into one-step catalytic conversion of ethanol to butadiene over bifunctional Zn-Y/Beta zeolite, ACS Catal. 8 (2018) 2760–2773.
[31] Z.W. Chen, Z. Li, Y. Zhang, D. Chevell, G.M. Li, Y.P. Chen, X.H. Guo, J. Liu, J.Q. Yu, A green route for the synthesis of nano-sized hierarchical ZSM-5 zeolite with excellent DTO catalytic performance, Chem. Eng. J. 388 (2020), 124322.
[32] E.H. Yuan, G.J. Wu, W.L. Dai, N.J. Guan, L.D. Li, One-pot construction of Fe/ZSM-5 zeolites for the selective catalytic reduction of nitrogen oxides by ammonia, Catal. Sci. Technol. 7 (2017) 3036–3044.
[33] E.H. Yuan, K. Zhang, G.X. Lu, Z.L. Mo, Z.C. Tang, Synthesis and application of metal-containing ZSM-5 for the selective catalytic reduction of NO_x with NH_3, J. Ind. Eng. Chem. 42 (2016) 142–148.
[34] T.D. Courtney, C.C. Chang, R.J. Gorte, R.F. Lobo, W. Fan, V. Nikolakis, Effect of water treatment on Sn-BEA zeolite: origin of 960 cm^{-1} FTIR peak, Microporous Mesoporous Mater. 210 (2015) 69–76.
[35] M.A. Camblor, A. Corma, J. Pérez-Pariente, Infrared spectroscopic investigation of titanium in zeolites. A new assignment of the 960 cm^{-1} band, J. Chem. Soc., Chem. Commun. (1993) 557–559.
[36] M. Signorile, V. Crocella, A. Damin, B. Rossi, C. Lamberti, F. Bonino, S. Bordiga, Effect of Ti speciation on catalytic performance of TS-1 in the hydrogen peroxide to propylene oxide reaction, J. Phys. Chem. C 122 (2018) 9021–9034.
[37] J.Q. Yan, G.J. Wu, N.J. Guan, L.D. Li, Nb_2O_5/TiO_2 heterojunctions: synthesis strategy and photocatalytic activity, Appl. Catal. B Environ. 152–153 (2014) 280–288.
[38] N. Candu, M.E. Fergani, M. Verziu, B. Cojocaru, B. Jurca, N. Apostol, C. Teodorescu, V.I. Parvulescu, S.M. Coman, Efficient glucose dehydration to HMF onto Nb-BEA catalysts, Catal. Today 325 (2019) 109–116.
[39] X.T. Gao, I.E. Wachs, M.S. Wong, J.Y. Ying, Structural and reactivity properties of Nb-MCM-41: comparison with that of highly dispersed Nb_2O_5/SiO_2 catalysts, J. Catal. 203 (2001) 18–24.
[40] M. Anilkumar, W.F. Hoelderich, A one step synthesis of caprolactam out of cyclohexanone by combined ammoximation and Beckmann rearrangement over Nb-MCM-41 catalysts, Appl. Catal. B Environ. 165 (2015) 87–93.
[41] I. Nowak, M. Jaroniec, Three-dimensional cubic mesoporous molecular sieves of FDU-1 containing niobium: dependence of niobium source on structural properties, Langmuir 21 (2005) 755–760.
[42] L.J. Burcham, J. Datka, I.E. Wachs, In situ vibrational spectroscopy studies of supported niobium oxide catalysts, J. Phys. Chem. B 103 (1999) 6015–6024.
[43] P. Yang, S.K. Fan, Z.Y. Chen, G.F. Bao, S.F. Zuo, C.Z. Qi, Synthesis of Nb_2O_5 based solid superacid materials for catalytic combustion of chlorinated VOCs, Appl. Catal. B Environ. 239 (2018) 114–124.
[44] S. Song, L. Di, G.J. Wu, W.L. Dai, N.J. Guan, L.D. Li, Meso-Zr-Al-beta zeolite as a robust catalyst for cascade reactions in biomass valorization, Appl. Catal. B Environ. 205 (2017) 393–403.
[45] S. Sumiya, Y. Oumi, M. Sadakane, T. Sano, Facile preparation of SBA-15-supported niobic acid (Nb_2O_5▪nH_2O) catalyst and its catalytic activity, Appl. Catal. Gen. 365 (2009) 261–267.
[46] Q. Zhao, W.H. Chen, S.J. Huang, Y.C. Wu, H.K. Lee, S.B. Liu, Discernment and quantification of internal and external acid sites on zeolites, J. Phys. Chem. B 106 (2002) 4462–4469.
[47] S. Lang, M. Benz, U. Obenaus, R. Himmelmann, M. Hunger, Novel approach for the characterization of Lewis acidic solid catalysts by solid-state NMR spectroscopy, ChemCatChem 8 (2016) 2031–2036.